Available online at www.sciencedirect.com
SCIENCE DIRECT
Journal of Catalysis 227 (2004) 367–374
JOURNAL OF CATALYSIS
www.elsevier.com/locate/jcat

Structure of active Ag clusters in Ag zeolites for SCR of NO by propane in the presence of hydrogen

Junji Shibata [a], Ken-ichi Shimizu [a,*], Yuu Takada [a], Akira Shichi [a], Hisao Yoshida [a], Shigeo Satokawa [b], Atsushi Satsuma [a], Tadashi Hattori [a]

[a] *Department of Applied Chemistry, Graduate School of Engineering, Nagoya University, Chikusa-ku, Nagoya 464-8603, Japan*
[b] *Tokyo Gas Co., Ltd., 1-16-25 Shibaura, Minato-ku, Tokyo 105-0023, Japan*

Received 6 July 2004; revised 5 August 2004; accepted 8 August 2004

Available online 3 September 2004

Abstract

The detailed structure of Ag clusters formed in H zeolites during H_2 reduction as well as under $NO + C_3H_8 + O_2 + H_2$ reaction condition is examined with H_2-TPR, XRD, UV–vis, and Ag *K*-edge XAFS. H_2-TPR results suggest a quantitative conversion of the exchanged Ag^+ ion to $Ag_2{}_p{}^{p+}$ cluster in Ag-MFI during H_2 reduction in a temperature range from 373 to 573 K. Combined with the UV–vis spectrum of the cluster, exhibiting bands at 255 and 305 nm, and Ag *K*-edge EXAFS result, the structure of the cluster is identified as $Ag_4{}^{2+}$. UV–vis and Ag *K*-edge XANES/EXAFS results reveal that, during $NO + C_3H_8 + O_2 + H_2$ reaction at 573 K, part of the Ag^+ ions are converted to $Ag_n{}^{\delta+}$ clusters, whose average structure can be close to $Ag_4{}^{2+}$. The amount of the clusters increases with the Ag/Al ratio of Ag zeolites. The NO reduction rate of Ag-MFI for the $NO + C_3H_8 + O_2$ reaction is significantly improved by an addition of 0.5% H_2, and the rate increases with Ag/Al ratio of Ag-MFI. This cluster does not form on Ag-MOR under the same conditions, and the NO reduction rate does not increase by H_2 addition. The structure–activity relationship shows that the $Ag_n{}^{\delta+}$, probably the $Ag_4{}^{2+}$ cluster, in Ag-MFI catalysts is responsible for the selective reduction of NO by C_3H_8.

Keywords: NO reduction; Ag zeolite; Cluster; Hydrogen

1. Introduction

Metal nanoparticles receive a great deal of attention in various fields including catalysis [1–3]. Among the metal clusters, many efforts have been devoted to study the formation and characterization of Ag clusters, and various types of Ag clusters in rare gas solids [4,5], in water [6–10], and in zeolites [3,11–24] have been reported to be formed by γ- or electron-ray irradiation, by reduction with reducing reagents, and by vacuum dehydration. Metallic and cationic clusters composed of 2–8 Ag atoms were typically proposed as Ag clusters in zeolites. Although the formation of Ag clusters has been discussed extensively [3,11–24], there are few reports demonstrating a specific catalysis of Ag clusters in zeolites for the reactions such as photocatalytic degradation of malathion [22], photo-dimerization of alkane [23,24], and methane conversion into propylene in the presence of ethylene [25]. Characterization of Ag clusters will lead to a molecular-level understanding of the relationship between properties of Ag nanoparticles and the catalytic performance. However, very few have succeeded in determining a detailed structure of the active Ag cluster. UV–vis measurement is widely used for a qualitative characterization of Ag clusters in zeolites [8–10,13–17]. Generally, the Ag cluster with the larger number of Ag atoms gives the UV–vis band of higher wavelength. However, there is inconsistency in the assignment of the bands. For example, Gachard et al. assigned absorption bands at 265 and 310 nm to $Ag_3{}^{2+}$ [15], whereas Ozin and Hugues assigned an ab-

* Corresponding author.
E-mail address: kshimizu@apchem.nagoya-u.ac.jp (K.-i. Shimizu).

0021-9517/$ – see front matter
doi:10.1016/j.jcat.2004.08.007

sorption band at 402 nm to the same Ag_3^{2+} [17]. On the other hand, Beyer and Jacobs [19] proposed, from a H_2-TPR result of Ag chabasites, that Ag clusters with uniform structure, $(Ag_2^+)_n$ and $(Ag_3^+)_m$, were formed under H_2-TPR conditions at about 370 and 473 K, respectively, though their local structure was not characterized in detail. A combination of a qualitative analysis by UV–vis and quantitative analyses with, for example, H_2-TPR and EXAFS is necessary to clarify the structure of the Ag cluster.

Recently, we have shown that the activity of Ag-exchanged zeolites for selective reduction of NO by C_3H_8 (C_3H_8-SCR) was significantly enhanced by the addition of 0.5% H_2 [20,21]. Ag clusters formed during the C_3H_8-SCR were characterized by UV–vis as a function of H_2 concentration and reaction time, and we found that Ag^+ ions were partly converted to $Ag_n^{\delta+}$ clusters by the addition of H_2. The results suggest a novel De-NO_x catalysis of $Ag_n^{\delta+}$ clusters for C_3H_8-SCR in the presence of H_2, although a further structural information of the $Ag_n^{\delta+}$ clusters is needed for a fundamental understanding of this novel catalytic system.

The objective of this study is first to establish structure of the model Ag clusters in the Ag-MFI sample by a combination of H_2-TPR, UV–vis and Ag *K*-edge XANES/EXAFS analyses. On the basis of a H_2-TPR, UV–vis, and Ag *K*-edge XAFS result, Ag-MFI after the H_2 reduction at a relatively low temperature (573 K) is given as a reference sample consisting mostly of the Ag_4^{2+} cluster. Next the structure of the $Ag_n^{\delta+}$ cluster formed under the $NO + C_3H_8 + O_2 + H_2$ reaction at 573 K is estimated by a comparison with the above reference sample. The relationship between the NO reduction rate and the relative amount of the $Ag_n^{\delta+}$ clusters is discussed as a function of Ag/Al ratio to show that the $Ag_n^{\delta+}$ cluster acts as active species in the reaction.

2. Experimental

Parent zeolites used in this study were H-MFI(13) (JRC-Z5-25H supplied from Catalysis Society of Japan, Si/Al = 13), H-MFI(22) (Tosoh-H-MFI supplied from Tosoh Co. Japan, Si/Al = 22), and NH_4^+-MOR(7.7) prepared by ion exchange of Na-MOR (Tosoh) with an aqueous NH_4NO_3 solution at 353 K for 18 h. Ag^+ ion-exchanged zeolites were prepared from H^+ or NH_4^+ form zeolites by ion exchange with an aqueous $AgNO_3$ solution at room temperature [26,27]. The prepared samples were filtered, rinsed with distilled water, and dried at 383 K, followed by calcination in flowing dried air at 773 K for 6 h. The calcined samples were analyzed by inductively coupled plasma emission spectroscopy (ICP, Jarrel-Ash Model 975) to determine their elemental composition. Table 1 shows the list of calcined Ag zeolites. Hereafter, the catalysts will be designated as Ag-zeolite type (Si/Al ratio)–Ag exchange level, e.g., Ag-MFI(22)-58.

H_2-TPR was carried out using H_2(7%)/Ar as a reducing gas (50 $cm^3\,min^{-1}$) at a heating rate of 10 K min^{-1}. Prior to the TPR experiment, catalysts were pretreated in a flow of O_2 at 773 K for 1 h, and then were cooled to room temperature in a flow of He. The change in the H_2 concentration was monitored with TCD. Water produced during the reduction process was removed in a U-shape stainless tube at 201 K (dry ice–ethanol) before entering the TCD.

Table 1
List of the Ag ion-exchanged zeolites used in the study

Catalyst[a]	Si/Al ratio	Ag/Al ratio	Overall Ag content	
			wt%	μmol g^{-1}
Ag-MFI(13)-30	13	0.30	3.5	290
Ag-MFI(22)-28	22	0.28	1.7	160
Ag-MFI(22)-48	22	0.48	3.0	280
Ag-MFI(22)-58	22	0.58	3.5	320
Ag-MOR(7.7)-33	7.7	0.33	5.4	500

[a] The catalysts is designated as Ag-zeolite type (Si/Al ratio)–Ag exchange level, e.g., Ag-MFI(13)-30.

Powder X-ray diffraction (XRD) was employed for detection of metallic Ag and Ag_2O crystallines on the catalyst after the treatment under the 7% H_2 flow. XRD patterns were obtained with Rigaku RINT 1200 using Cu-K_α radiation filtered by Ni. Diffuse reflectance UV–vis spectra of catalysts were measured with JASCO V-570. The sample was exposed to various gas mixtures at 573 K for 0.5 h and quenched at room temperature. Then, UV–vis spectra of the quenched sample were measured after moving into an optical quartz cell without exposure to the air.

Ag *K*-edge XAFS spectra were recorded at the BL-10B station at KEK-PF with a Si(311) channel-cut monochrometer in transmission mode at room temperature. The incident and transmitted X-rays were monitored by ionization chambers filled with Ar gas, with the length of 17 and 62 cm. The catalysts exposed to various gas mixtures at 573 K for 0.5 h were cooled to room temperature in a flow of helium and were sealed in cells made of borosilicate. The thickness of the cell was chosen to be 4–5 mm to give an edge jump around 0.4–1.0. Normalization of XANES and data reduction on EXAFS were carried out as described elsewhere [28] using XAPEC4. The Fourier transforms of k^3-weighted Ag *K*-edge EXAFS spectra were obtained in the *k* range of 4–11 $Å^{-1}$. The back Fourier filtered data were analyzed by a usual curve-fitting method based on

$$\chi(k) = \sum \frac{N_j}{kr_j^2} F_j(k) \exp\left(-2k_j^2 \Delta(\sigma_j^2)\right) \times \sin\left(2kr_j + \delta_j(k)\right), \quad (1)$$

where N_j, r_j, and $\Delta(\sigma_j)^2$ represent the coordination number, the bond distance, and the Debye–Waller factor, respectively. $F_j(k)$ and $\delta_j(k)$ represent amplitude and phase-shift functions, respectively. For the curve-fitting analysis, the empirical phase shift and amplitude functions for Ag–O and Ag–Ag were extracted from the data for Ag_2O and Ag foil, respectively. Errors in the analysis were estimated by

residual factor (R_f) determined by

$$R_f = \int \left|k^3\chi^{obs}(k) - k^3\chi^{calc}(k)\right|^2 dk \Big/ \int \left|k^3\chi^{obs}(k)\right|^2 dk. \quad (2)$$

3. Results and discussion

3.1. Structural analysis of stable clusters formed during reduction of Ag species by H_2

H_2-TPR results by Beyer and Jacobs [19] suggest the synthesis of a Ag-zeolite sample composed of a single Ag cluster. They reported that Ag clusters with uniform structure, $(Ag_2^+)_n$ and $(Ag_3^+)_m$, were formed on Ag chabasites under H_2-TPR conditions at about 370 and 473 K, respectively. Fig. 1 shows H_2-TPR profiles of Ag zeolites. For Ag-MFI samples, there were two H_2 consumption peaks, and the first peak appeared at a temperature range from 373 to 573 K. The temperature of the second peak was shifted to a lower temperature with an increase in Ag content. On Ag-MOR, H_2 desorption was observed from 600 to 850 K and reduction of this sample was not completed at 1023 K, as reported by Berndt et al. [29].

The amount of H_2 consumed and H_2/Ag ratio at the first and the second peaks are shown in Table 2. For all the Ag-MFI samples, H_2/Ag ratios of the first and the second peaks were quite close to each other and were estimated to be about 0.25. The following two hypotheses can explain the above result: (1) Half of Ag^+ ions are reduced to Ag metal particles or metallic Ag clusters at the first peak, and the remaining Ag^+ ions are reduced to Ag metal particles at the second peak. (2) All of Ag^+ ions are reduced to $Ag_{2p}{}^{p+}$ clusters at the first peak, and the $Ag_{2p}{}^{p+}$ clusters are reduced to Ag metal particles at the second peak. Possibility (1) may be valid if reducibility of Ag^+ ion depends strongly on ion-exchanged sites. It is well established that the metal cation distribution at various ion-exchanged sites depends on metal loading [30]. Hence, the H_2/Ag ratio of the first and the second peaks should depend on the Ag/Al ratio if possibility (1) is valid, though the result in Table 2 is inconsistent with this possibility. XRD patterns of Ag-MFI(22)-58 treated at various temperatures in flowing H_2 were compared in Fig. 2. All diffraction lines observed in the sample after O_2 treatment (pattern a) were assigned to MFI zeolite. No diffraction

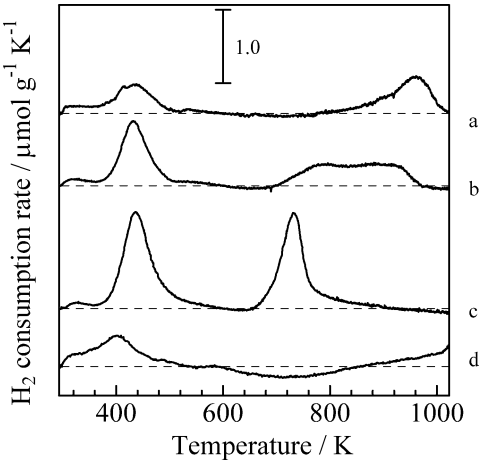

Fig. 1. H_2-TPR profiles of (a) Ag-MFI(22)-28, (b) Ag-MFI(22)-48, (c) Ag-MFI(22)-58, and (d) Ag-MOR(7.7)-33.

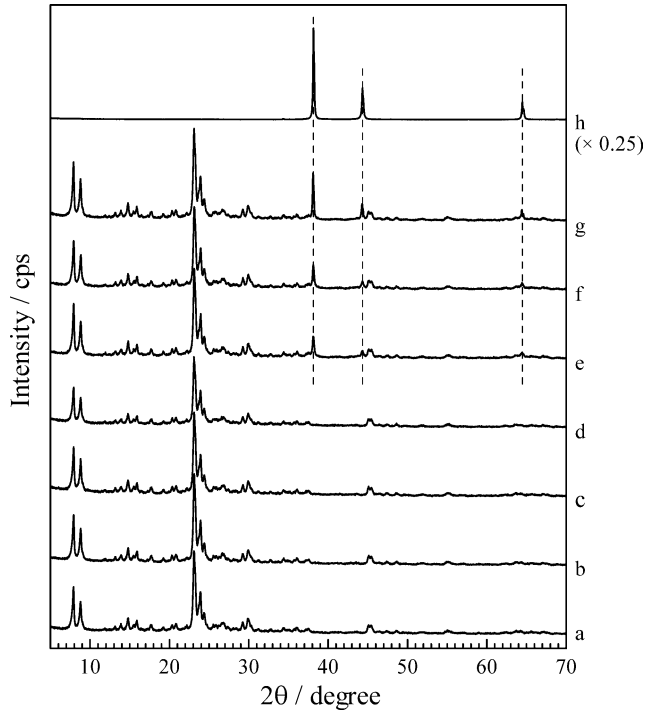

Fig. 2. XRD patterns of Ag-MFI(22)-58 after a flow of (a) O_2 at 773 K for 1 h and 7% H_2 at (b) 373, (c) 473, (d) 573, (e) 673, (f) 773, and (g) 873 K for 30 min. This figure includes a pattern of (h) Ag metal powders.

Table 2
H_2 amount consumed in H_2-TPR of Ag zeolites

Samples	Overall Ag content (μmol g^{-1})	First peak		Second peak		Sum of H_2/Ag at first and second peaks
		Consumed H_2 (μmol g^{-1})	H_2/Ag	Consumed H_2 (μmol g^{-1})	H_2/Ag	
Ag-MFI(22)-28	160	38	0.24	47	0.30	0.54
Ag-MFI(22)-48	280	66	0.24	76	0.27	0.51
Ag-MFI(22)-58	320	85	0.26	87	0.27	0.53
Ag-MOR(7.7)-33	500	50	0.10	> 33[a]	> 0.07[a]	> 0.11[a]

[a] The reduction is not completed.

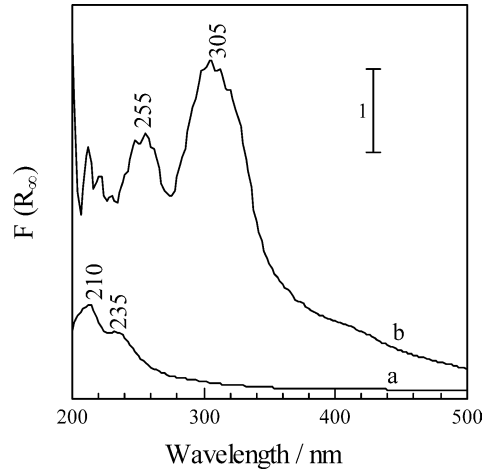

Fig. 3. UV–vis spectra of Ag-MFI(22)-58 (a) after treating in a flow of 10% O_2 at 773 K for 1 h and (b) in a flow of 0.5% H_2 at 573 K for 0.5 h.

lines due to metallic Ag crystallites ($2\theta = 38.1$, 44.3, and 64.5°) appeared after the H_2 treatment below 573 K (patterns b–d) where a second reduction did not occur in the H_2-TPR (Fig. 1c). Formation of metallic Ag was observed after the H_2 treatment above 673 K (patterns e–f) where a second reduction started. This result confirms that possibility (1) is excluded, and thus H_2-TPR suggests that all of Ag^+ ions are reduced to $Ag_{2p}{}^{p+}$ clusters at the end of the first peak (around 573 K).

The following results show the structure of Ag-MFI after a H_2 reduction at 573 K, where most of the Ag species should be present as the $Ag_{2p}{}^{p+}$ cluster. Fig. 3 shows UV–vis spectra of Ag-MFI(22)-58 before and after the H_2 treatment. After the pretreatment in a flow of 10% O_2 at 773 K (spectrum a), bands at 210 and 235 nm assignable to the $4d^{10}$ to $4d^9s^1$ transition of Ag^+ ion [20,31,32] were observed. After the H_2 treatment at 573 K, strong bands around 255 and 305 nm were observed (spectrum b). The positions of these bands are close to those reported by Gachard et al. who assigned the UV absorption bands at 265 and 310 nm to $Ag_3{}^{2+}$ [15]. In the study on γ-irradiated Ag–Cs-rho zeolites, Michalik et al. assigned the absorption band at 270 nm to $Ag_4{}^{2+}$ [13]. Considering the H_2-TPR result suggesting the formation of the $Ag_{2p}{}^{p+}$ cluster below 573 K, the bands at 255 and 305 nm can be tentatively assigned to the $Ag_4{}^{2+}$ cluster. Note that bands around 350–480 nm due to small Ag metal particles [20,33,34] were very weak and broad. Combined with the result that diffraction lines due to metallic Ag crystallites did not appear in the sample treated under the same conditions (Fig. 2d), it is obvious that Ag metal particles are minor species. Ag K-edge XAFS spectra were measured to determine the detailed structure of the $Ag_{2p}{}^{p+}$ cluster, particularly number of atoms in the $Ag_{2p}{}^{p+}$ cluster. Fig. 4A shows XANES spectra of Ag-MFI(22)-58 before (spectrum i) and after (spectrum e) the H_2 treatment at 573 K together with those of Ag metal, Ag_2O and Ag_2SO_4. Ag_2SO_4 consists of Ag^+ ions surrounded by six oxygens with Ag–O bond distances of 2.4–2.6 Å [35], and

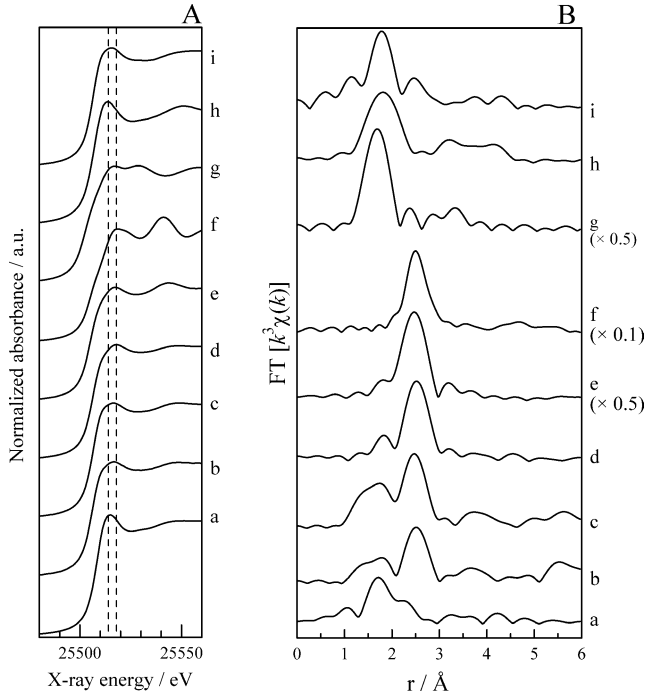

Fig. 4. (A) Ag K-edge XANES spectra and (B) Fourier transforms of k^3-weighted EXAFS spectra of (a) Ag-MOR(7.7)-33, (b) Ag-MFI(13)-30, (c) Ag-MFI(22)-48, and (d) Ag-MFI(22)-58 after a flow of NO + C_3H_8 + O_2 + H_2 at 573 K, (e) Ag-MFI(22)-58 after a flow of 0.5% H_2 at 573 K, (f) Ag foil, (g) Ag_2O, (h) Ag_2SO_4, and (i) Ag-MFI(22)-58 after a flow of 10% O_2 at 773 K for 1 h.

thus, it can be regarded as a reference compound for ionic Ag^+ species surrounded by oxygens. The XANES feature of Ag-MFI(22)-58 after the oxidation at 773 K was close to that of Ag_2SO_4, suggesting that Ag species in this sample are present as Ag^+ ions. After H_2 treatment at 573 K, the XANES feature of Ag-MFI(22)-58 changed and was rather similar to that of Ag foil, although the peak at 25518 eV, characteristic of Ag foil, was broader for Ag-MFI(22)-58 after the reduction. It is clear that the $Ag_{2p}{}^{p+}$ cluster, which is the predominant Ag species after the H_2 reduction at 573 K, gives different spectral features from Ag metal, Ag_2O and Ag^+ ion-exchanged to the zeolite.

Fig. 4B shows Fourier transform of k^3-weighted EXAFS spectra of Ag-MFI(22)-58 before and after the H_2 treatment. A peak at 1.7 Å due to the Ag–O shell, observed before the reduction (spectrum i), disappeared after the reduction (spectrum e) and a new peak at 2.5 Å assignable to the Ag–Ag shell was observed. The position of the latter peak was shorter than that of the Ag–Ag shell of Ag foil (2.7 Å). The inverse Fourier transform of this new peak at 2.5 Å ($R = 2.0$–3.0 Å) in spectrum e in Fig. 4B gives the EXAFS oscillation due to the Ag–Ag as shown in Fig. 5 (spectrum e) with a solid line. The dotted line in Fig. 5 shows the result of a curve-fitting analysis using Ag–Ag shell parameters in the k region of 4.0–11.0 Å $^{-1}$. A simulated spectrum fitted well with the experimental one. As shown in Table 3, the curve-fitting analysis of the peak at 2.5 Å showed that this peak

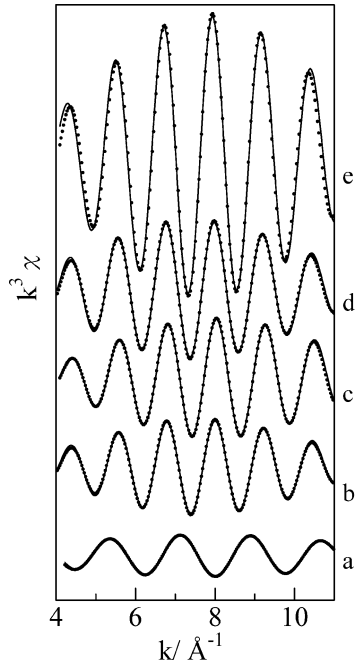

Fig. 5. Fourier-filtered EXAFS function (solid line) and resulting curve fit (dotted line) for the main peak appearing at 1.0–2.0 Å (a) or at 2.0–3.0 Å (b–e) in FT of k^3-weighted EXAFS (spectra a–e in Fig. 4B): (a) Ag-MOR(7.7)-33, (b) Ag-MFI(13)-30, (c) Ag-MFI(22)-48, (d) Ag-MFI(22)-58 after a flow of NO + C_3H_8 + O_2 + H_2 at 573 K, and (e) Ag-MFI(22)-58 after a flow of 0.5% H_2 at 573 K.

Table 3
Curve-fitting analysis of Fourier-transformed EXAFS of various Ag zeolites after C_3H_8-SCR in the presence of 0.5% H_2

Samples	Scatter arom	N[a]	r[b] (Å)	$\Delta(\sigma^2)$[c] (Å^2)	R_f[d] (%)
Ag-MFI(22)-48	Ag	1.3	2.71	8.93×10^{-4}	5.0
Ag-MFI(22)-58	Ag	1.9	2.73	3.34×10^{-3}	5.0
Ag-MFI(13)-30	Ag	1.0	2.72	1.46×10^{-3}	4.7
Ag-MOR(7.7)-33	O	0.9	2.11	6.63×10^{-3}	13.3
Ag-MFI(22)-58 after H_2 treatment at 573 K	Ag	3.3	2.73	1.91×10^{-3}	5.3
Ag foil[e]	Ag	(12)	(2.89)		
Ag_2O[e]	O	(2)	(2.04)		

[a] Coordination number.
[b] Bond distance.
[c] Debye–Waller factor.
[d] Residual factor.
[e] Data from X-ray crystallography.

can be assigned to Ag–Ag shell with a coordination number of 3.3 and bond distance 2.73 Å. These values are smaller than those of Ag foil: coordination number 12 and distance 2.89 Å. Monsanto et al. have reported that the Ag–Ag distance of the Ag_2 cluster in solid Ar matrix is 2.5 Å [5]. In the ESR study on the Ag cluster in AgNa-Y, Xu and Kevan assumed an Ag–Ag distance of Ag_4 clusters of 2.7 Å [18]. Kim and Seff reported that the Ag–Ag distance of the Ag_6^{n+} cluster was 2.92 Å with XRD [11]. Compared with the above literature data, the coordination number 3.3 and the Ag–Ag distance around 2.7 Å for Ag_{2p}^{p+} cluster (Table 3) suggest that the cluster consists of 3–4 Ag atoms. Summarizing the H_2-TPR, UV–vis, and XAFS results, we conclude that the most probable structure of the Ag_{2p}^{p+} cluster formed by the H_2 reduction of Ag-MFI at 573 K is Ag_4^{2+}.

3.2. Structure of Ag cluster formed under SCR

For Ag zeolites listed in Table 1, the structure of Ag clusters formed under the C_3H_8-SCR condition (NO = 1000 ppm, C_3H_8 = 1000 ppm, O_2 = 10%, and H_2 = 0 or 0.5%) at 573 K was examined with various spectroscopic methods. For all the samples, XRD showed no diffraction lines due to metallic Ag crystallites after a flow of NO + C_3H_8 + O_2 at 573 K both in the absence and in the presence of 0.5% H_2. The UV–vis spectrum of each Ag-zeolite samples obtained after the C_3H_8-SCR reaction at 573 K in the absence of H_2 (result not shown) was very close to that obtained after the oxidation at 773 K (spectrum a in Fig. 3); bands assignable to the $4d^{10}$ to $4d^9s^1$ transition of Ag^+ ion (around 210–240 nm) were observed, and no band due to metallic Ag species at a higher wavelength region was observed. This indicates that Ag^+ ions are the predominant Ag species before the reaction and under the C_3H_8-SCR reaction conditions at 573 K. Fig. 6 shows UV–vis spectra after the NO + C_3H_8 + O_2 reaction in the presence of 0.5% H_2 for 0.5 h. On Ag-MOR (spectrum a), bands due to Ag^+ ion (around 210–240 nm) were mainly observed, which indicates that Ag^+ ions are the predominant Ag species even under the presence of 0.5% H_2. On the other hand, the UV–vis spectra of Ag-MFI samples changed by the addition of H_2 in the reaction feed, and new bands at 260 and 285 nm were observed (spectra b–e). The position of these bands is close to those of the Ag_4^{2+} cluster (Fig. 3b, 255 and 305 nm) assigned in the above section. Henglein and co-workers assigned the absorption band around 280 nm to Ag_4^{2+} in the studies on pulse radiolytic reduction of Ag ions in aqueous solution [8–10]. Michalik et al. assigned the absorption band at 282 nm to Ag_4^{3+} in the γ-irradiated Ag-containing zeolite [13]. Gachard et al. reported the formation of Ag_3^{2+} (265 nm) through γ-irradiation to AgNa-Y zeolites [15]. Taking into account these literature data, we have assigned these bands to $Ag_n^{\delta+}$ cluster ($2 < n < 4$) in our previous study [20]. The band intensities change in the order of Ag-MFI(22)-58 > Ag-MFI(22)-48 > Ag-MFI(13)-30. This result indicate that $Ag_n^{\delta+}$ clusters with similar structures are present on all Ag-MFI samples after the reaction, and the amount of the cluster increases with Ag/Al ratio.

Detailed structure of $Ag_n^{\delta+}$ cluster was determined by Ag K-edge XAFS spectra. Fig. 4A includes XANES spectra of Ag zeolites after the NO + C_3H_8 + O_2 + H_2 reaction at 573 K. Fourier transforms of k^3-weighted EXAFS spectra of the samples are shown in Fig. 4B. The XANES feature of Ag-MOR(7.7)-33 (spectrum a), having a peak at 25514 eV, is very close to that of Ag_2SO_4. In the EXAFS spectrum of Ag-MOR(7.7)-33, only a peak due to Ag–O shell at 1.7 Å

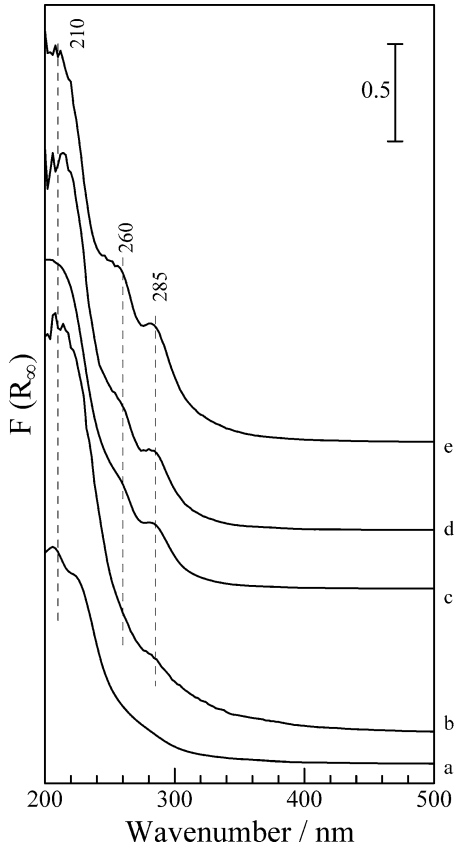

Fig. 6. UV–vis spectra of the Ag zeolites after a flow of NO + C_3H_8 + O_2 + H_2 at 573 K: (a) Ag-MOR(7.7)-33, (b) Ag-MFI(13)-30, (c) Ag-MFI(22)-28, (d) Ag-MFI(22)-48, and (e) Ag-MFI(22)-58.

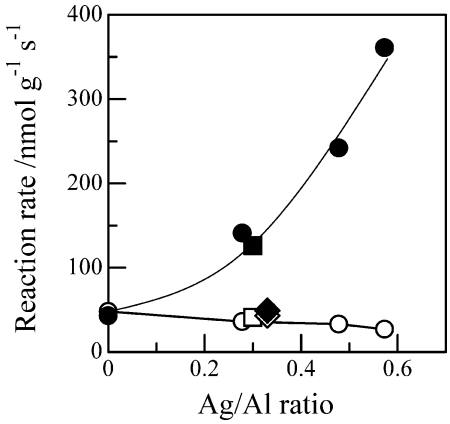

Fig. 7. NO reduction rate versus Ag/Al ratio for the C_3H_8-SCR over Ag-MFI(22) samples with various Ag loading (○, ●), Ag-MFI(13)-30 (□, ■), and Ag-MOR(7.7)-33 (◊, ♦) in the (open symbols) absence and (closed symbols) in the presence of 0.5% H_2 at 573 K.

was observed (spectrum a). These results indicate that Ag^+ ions are predominant on Ag-MOR, which agrees with the UV–vis result (spectrum a in Fig. 6). The XANES feature of Ag-MFI samples (spectra b–d), having a peak at 25518 eV, is rather similar to that of Ag-MFI(22)-58 after the H_2 treatment at 573 K consisted mainly of the Ag_4^{2+} cluster (spectrum e). In the EXAFS spectra of Ag-MFI (spectra b–d), the peak at 2.5 Å is observed, and its position is the same as that of the Ag–Ag shell of the Ag_4^{2+} cluster (spectrum e). Fig. 5 shows the inverse Fourier transforms of the Ag–Ag shell at 2.5 Å for Ag-MFI samples (the spectra b–d in Fig. 4B) or the Ag–O shell at 1.7 Å for Ag-MOR (the spectrum a in Fig. 4B) with solid lines. The dotted lines in Fig. 5 show the result of curve-fitting analyses in the k region of 4.0–11.0 $Å^{-1}$ using Ag–Ag shell parameters for Ag-MFI samples (the spectra b–d) or Ag–O shell parameters for Ag-MOR (the spectrum a). The result of the curve-fitting analysis (Table 3) confirmed that the peak at 2.5 Å, observed on Ag-MFI samples after the reaction, is assigned to the Ag–Ag shell with a distance of 2.72 ± 0.01 Å, which is almost the same as that of Ag-MFI(22)-58 after H_2 treatment (Ag_4^{2+} cluster). Taking into account a significant influence of the cluster size on Ag–Ag bond distances reported in the literature [5,11,18] discussed in the above section, the EXAFS result suggests that the $Ag_n^{\delta+}$ cluster consists of four Ag atoms. The coordination number of Ag–Ag shell on Ag-MFI(22)-58 after the reaction was estimated to be 1.9. Note that the UV–vis result in Fig. 6 indicates that both Ag^+ ions and $Ag_n^{\delta+}$ clusters, having the bands at 260 and 285 nm irrespective of the Ag/Al ratio, are present on all Ag-MFI samples during the reaction. Therefore, it is reasonable to assume that the Ag–Ag coordination numbers of these samples (Table 3) are lower than those of $Ag_n^{\delta+}$ clusters in the samples. From the above considerations, we propose that the main $Ag_n^{\delta+}$ cluster formed during the NO + C_3H_8 + O_2 + H_2 reaction is mainly Ag_4^{2+}. Considering the fact that the reaction condition (NO = 1000 ppm, C_3H_8 = 1000 ppm, O_2 = 10%, and H_2 = 0.5%) is in a more oxidizing atmosphere than the condition used to prepare Ag_4^{2+} clusters (10% H_2/He), one might assume that the $Ag_n^{\delta+}$ cluster is amore cationic species than the Ag_4^{2+} cluster. Hence, the presence of minor species such as Ag_4^{3+}, Ag_2^{+}, and Ag_3^{2+} may not be excluded. The cluster size of Ag_4^{2+} is estimated as 5.4 Å according to the report by Xu and Kevan [18]. This size is close to the pore diameter of MFI (5.3 × 5.6 Å in main channel [36]), which suggests that the $Ag_n^{\delta+}$ cluster is located in the channel of MFI. As the Ag/Al ratio in Ag-MFI increased, the coordination number of the Ag–Ag shell increased, which is consistent with the UV–vis results that the intensity of the bands due to the $Ag_n^{\delta+}$ cluster (260 and 285 nm) increased with Ag/Al ratio. These results indicate that the amount of the $Ag_n^{\delta+}$ clusters, probably Ag_4^{2+} clusters, increases with Ag/Al ratio.

3.3. Structure–activity relationship

The NO reduction rates per gram of the catalyst for NO + C_3H_6 + O_2 reaction were measured at 573 K in the absence and the presence of 0.5% H_2 with a series of catalysts characterized in the above section (Fig. 7). In the absence of H_2, the Ag zeolites showed slightly lower activity than H^+-exchanged zeolite, H-MFI(22), and the activity slightly decreased with an increase in the Ag/Al ratio. The presence

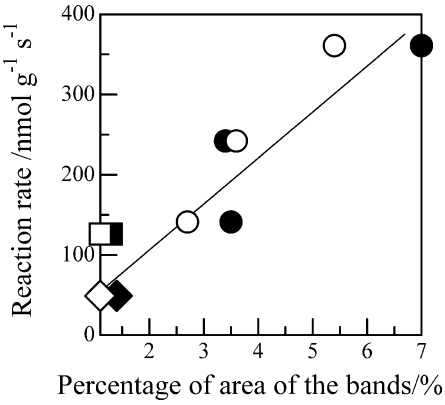

Fig. 8. NO reduction rate at 573 K in the presence of 0.5% H_2 for the C_3H_8-SCR over Ag-MFI(22) samples with various Ag loading (○, ●), Ag-MFI(13)-30 (□, ■), and Ag-MOR(7.7)-33 (◊, ♦) as a function of percentage of the bands due to $Ag_n^{\delta+}$ clusters: 260 nm (closed symbols) and 285 nm (open symbols). The percentage of the bands was estimated by deconvolution of each spectrum into subbands centered at 210, 230, 260, and 285 nm applying lineshape functions of Gaussian/Lorentzian = 2/8.

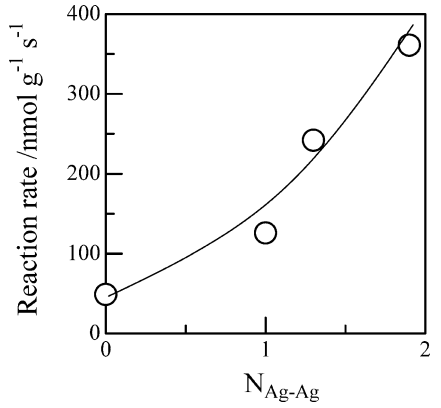

Fig. 9. NO reduction rate at 573 K in the presence of 0.5% H_2 for the C_3H_8-SCR on various Ag zeolites as a function of the coordination number of Ag–Ag shell due to $Ag_n^{\delta+}$ cluster.

of 0.5% H_2 increased the rates of NO reduction, and the rates increased with Ag/Al ratio. Whereas, the addition of H_2 did not increase the activity of Ag-MOR(7.7)-33. Fig. 8 shows the correlation between the relative intensity of the UV–vis bands due to the $Ag_n^{\delta+}$ cluster (260 and 285 nm) formed in the $NO + C_3H_6 + O_2 + H_2$ reaction (Fig. 5) and the NO reduction rate at 573 K in the presence of H_2. The results clearly indicate that the activity correlates well with the amount of $Ag_n^{\delta+}$ cluster.

As noted above, the characterization results suggest that the $Ag_n^{\delta+}$ with the same structure, probably Ag_4^{2+}, is predominant on all Ag-MFI samples during the reaction. It follows that the coordination number for the Ag–Ag shell (Table 3) should be proportional to the amount of $Ag_n^{\delta+}$ cluster. In Fig. 9, the NO reduction rate is plotted as a function of the coordination number of the Ag–Ag shell due to the cluster. Again, the result indicates that the activity correlates well with the amount of $Ag_n^{\delta+}$ cluster. From these results, it is concluded that the $Ag_n^{\delta+}$ cluster, probably the Ag_4^{2+} cluster, in Ag-MFI catalysts is responsible for the selective reduction of NO by C_3H_8.

4. Conclusion

Ag clusters are formed in Ag-MFI zeolites by the H_2 reduction of the exchanged Ag^+ ions in a temperature range from 373 to 573 K. Detailed characterization with H_2-TPR, UV–vis and Ag *K*-edge XAFS shows that the cluster is identified to be a Ag_4^{2+} cluster. UV–vis and Ag *K*-edge XAFS revealed that, during the $NO + C_3H_8 + O_2 + H_2$ reaction at 573 K, the exchanged Ag^+ ion is converted to the $Ag_n^{\delta+}$ cluster, and its amount increases with Ag/Al ratio. The structure of the cluster is estimated to be Ag_4^{2+} cluster. The structure–activity relationship shows that the $Ag_n^{\delta+}$ (Ag_4^{2+}) cluster in Ag-MFI catalysts is responsible for the selective reduction of NO by C_3H_8.

Acknowledgments

The X-ray absorption experiment was performed under the approval of the Photon Factory Program Advisory Committee (Proposal No. 2001G094). This work was partly supported by a Grant-in-Aid from the Ministry of Education, Science, and Culture, Japan. The authors thank Dr. K. Itabashi of Tosoh Co. for providing zeolite samples.

References

[1] G. Schmid, M. Bäumle, M. Geerkens, I. Heim, C. Osemann, T. Sawitowski, Chem. Soc. Rev. 28 (1999) 179.
[2] L.N. Lewis, Chem. Rev. 93 (1993) 2693.
[3] T. Sun, K. Seff, Chem. Rev. 94 (1994) 857.
[4] G.A. Ozin, H. Huber, Inorg. Chem. 17 (1978) 155.
[5] P.A. Montano, J. Zhao, M. Ramanathan, G.K. Shenoy, W. Schulze, J. Urban, Chem. Phys. Lett. 164 (1989) 126.
[6] T. Linnert, P. Mulvaney, A. Henglein, H. Weller, J. Am. Chem. Soc. 112 (1990) 4657.
[7] M. Mostafavi, M. Lin, G. Wu, Y. Katsumura, Y. Muroya, J. Phys. Chem. A 106 (2002) 3123.
[8] P. Mulvaney, A. Henglein, J. Phys. Chem. 94 (1990) 4182.
[9] T. Linnert, P. Mulvaney, A. Henglein, H. Weller, J. Am. Chem. Soc. 112 (1990) 4657.
[10] B.G. Ershov, E. Janata, A. Henglein, J. Phys. Chem. 97 (1993) 339.
[11] Y. Kim, K. Seff, J. Am. Chem. Soc. 100 (1978) 6989.
[12] S.Y. Kim, Y. Kim, K. Seff, J. Phys. Chem. B 107 (2003) 6938.
[13] J. Michalik, J. Sadlo, T. Kodaira, S. Shimomura, H. Yamada, J. Radioanal. Nucl. Chem. 232 (1998) 135.
[14] D.R. Brown, L. Kevan, J. Phys. Chem. 90 (1986) 1129.
[15] E. Gachard, J. Belloni, M.A. Subramanian, J. Mater. Chem. 6 (1996) 867.
[16] G.A. Ozin, M.D. Baker, J. Godber, J. Phys. Chem. 88 (1984) 4902.
[17] G.A. Ozin, F. Hugues, J. Phys. Chem. 87 (1983) 94.
[18] B. Xu, L. Kevan, J. Phys. Chem. 95 (1991) 1147.
[19] H.K. Beyer, P.A. Jacobs, Stud. Surf. Sci. Catal. 12 (1982) 95.

[20] J. Shibata, Y. Takada, A. Shichi, S. Satokawa, A. Satsuma, T. Hattori, J. Catal. 222 (2004) 368.
[21] J. Shibata, Y. Takada, A. Shichi, S. Satokawa, A. Satsuma, T. Hattori, Appl. Catal. B, in press.
[22] S.M. Kanan, M.C. Kanan, H.H. Patterson, J. Phys. Chem. B 105 (2001) 7508.
[23] G.A. Ozin, F. Hugues, J. Phys. Chem. 86 (1982) 5174.
[24] H. Yoshida, T. Hamajima, Y. Kato, J. Shibata, A. Satsuma, T. Hattori, Res. Chem. Intermed. 29 (2003) 897.
[25] T. Baba, H. Sawada, T. Takahashi, M. Abe, Appl. Catal. A 231 (2002) 55.
[26] Z. Li, M. Flytzani-Stephanopoulos, Appl. Catal. A 165 (1997) 15.
[27] Z. Li, M. Flytzani-Stephanopoulos, J. Catal. 182 (1999) 313.
[28] T. Tanaka, H. Yamashita, R. Tsuchitani, T. Funabiki, S. Yoshida, J. Chem. Soc., Faraday Trans. 1 84 (1988) 2987.
[29] H. Berndt, M. Richter, T. Gerlach, M. Baerns, J. Chem. Soc., Faraday Trans. 94 (1998) 2043.
[30] J. Dědeček, D. Kaucký, B. Wichterlová, Micropor. Mesopor. Mater. 35–36 (2000) 483.
[31] M. Matsuoka, E. Matsuda, K. Tsuji, H. Yamashita, M. Anpo, J. Mol. Catal. A 107 (1996) 399.
[32] J. Texter, T. Gonsiorowski, R. Kellerman, Phys. Rev. B 23 (1981) 4407.
[33] K.A. Bethke, H.H. Kung, J. Catal. 172 (1997) 93.
[34] N. Bogdanchikova, F.C. Meunier, M. Avalos-Borja, J.P. Breen, A. Pestryakov, Appl. Catal. B 36 (2002) 287.
[35] N.E. Brese, M. O'keeffe, B.L. Ramakrishna, R.B. Von Dreele, J. Solid State Chem. 89 (1990) 184.
[36] Ch. Baerlocher, W.M. Meier, D.H. Olson, Atlas of Zeolite Framework Types, Fifth Rev. ed., Elsevier, Amsterdam, 2001, p. 184.